

Deep Learning for EBG-Structured Microstrip Patch Antenna Optimization

Akash Chandra*, Aman Pathak*, SKS Parashar†

*School of Computer Engineering,

Kalinga Institute of Industrial Technology (KIIT), Deemed to be University
Bhubaneshwar - 751024, Odisha, India

Email: apathakcse@gmail.com

†Nanosensor Lab, School of Applied Sciences,

Kalinga Institute of Industrial Technology (KIIT), Deemed to be University
Bhubaneshwar - 751024, Odisha, India

Email: sksparasharfpv@kiit.ac.in, sksparashar@yahoo.com

Abstract—This paper explores the feasibility of utilizing Deep Neural Networks (DNN) for analyzing terahertz (THz) antennas, specifically EBG patterned microstrip patch antennas. Conventional design methods face difficulties in complexity and time requirements as the demand for smaller antennas working in the THz band increases. To tackle this challenge, we explore the utilization of Deep Neural Network (DNN) models to accelerate the process of design and optimize antenna efficiency. Our results demonstrate the effectiveness of NN models in forecasting antenna behavior and optimizing performance. In our design, we achieved a return loss (S11) of -59 dB, a gain of 6.04 dB, and a voltage standing wave ratio (VSWR) of 1.02. By applying the DNN model to our design, We attained a remarkable precision of 98%, accompanied by a negligible error margin of merely 0.05%. Furthermore, we compared our NN model with other machine learning models and found that it outperforms them in terms of accuracy and reliability. The benefits of utilizing DNN models in THz antenna design are twofold. Firstly, they enable rapid design and optimization, reducing the time and complexity associated with conventional methods. Secondly, they facilitate improved performance optimization, leading to enhanced antenna performance. These advantages have significant implications for the development of THz communication and sensing technologies.

Keywords— Neural Networks, Microstrip patch antennas, THz communication, Performance prediction, Machine Learning

I. INTRODUCTION

The development of microstrip patch antennas has seen a notable paradigm shift in recent years, as the need for high-performance wireless communication systems continues to grow. One of the key challenges in antenna design is the need to balance competing performance metrics, such as gain, directivity, and bandwidth, while also minimizing size and cost. To address this challenge, researchers have turned to Electromagnetic Band Gap (EBG) structures [1] [2], which have been shown to enhance antenna performance by mitigating limitations such as mutual coupling, surface wave excitation, and impedance mismatch[3][4].

EBG structures are periodic arrangements of metallic or dielectric elements that can be integrated into the antenna design to modify the electromagnetic properties of the surrounding environment. By carefully designing the EBG structure, it is possible to create a "defect" in the bandgap, allowing the antenna to operate at a specific frequency while rejecting other frequencies. This approach has been shown to improve antenna performance, enabling the development of compact, high-gain, and high-directivity antennas that are suitable for a wide range of applications, including wireless communication systems, radar, and sensing[5][6][7].

However, the optimization of EBG-structure based patch antennas remains a complex task, requiring the careful consideration of multiple parameters and their intricate interactions. Traditional design approaches, such as finite-element methods and genetic algorithms, can be time-consuming and computationally intensive, making it difficult to explore the vast design space and identify optimal solutions[8].

In recent years, machine learning (ML) models have emerged as a promising solution for tackling this complexity, offering a data-driven approach to antenna design that can uncover hidden patterns and relationships in the data. By training ML models on large datasets of antenna designs and performance metrics, it is possible to develop predictive models that can rapidly identify optimal designs and accelerate the antenna design process[9][10].

Among the various ML models available, deep neural networks (DNNs) have shown particular promise in the field of antenna design, thanks to their ability to learn complex representations of data and make accurate predictions. DNNs have been used to model a wide range of antenna design tasks, including antenna geometry optimization, frequency selection, and performance prediction[11]. However, the choice of DNN architecture and training parameters can significantly impact the performance of the model, and the optimal approach for microstrip EBG-structure based patch antenna design remains unclear.

This study aims to address this knowledge gap by conducting a comprehensive comparative analysis of different machine learning models, including DNNs, for microstrip EBG-structure based patch antenna design. By evaluating the performance of various models on a range of antenna design tasks, this study seeks to identify the best fit for this application and provide insights into the strengths and limitations of each approach[12]. The results of this study have the potential to accelerate the development of high-performance EBG-structure based patch antennas, enabling the realization of advanced wireless communication systems and other applications that rely on efficient and reliable antenna technology.

II. ANTENNA DESIGN REQUIREMENTS

The Antenna contains certain fundamental parameters which can be approximately estimated for a first run. The frequency of Operation is given by[13]

$$f_c \approx \frac{c}{2L\sqrt{\epsilon_r}} = \frac{1}{2L\sqrt{\epsilon_0\epsilon_r\mu_0}}$$

- f_c : This represents the cut-off frequency of the antenna in Hertz (Hz).
- c : This notation represents the speed of light in vaccum, which is roughly 3×10^8 meters per second (m/s) [14].
- L : This represents the length of the antenna in meters (m).

- ϵ_r : This represents the relative permittivity of the dielectric material used in the antenna.
- ϵ_0 : This represents the permittivity of free space, which is a constant value of approximately 8.85×10^{-12} Farads per meter (F/m) [14].
- μ_0 : This represents the permeability of free space, which is another constant value of approximately $4\pi \times 10^{-7}$ Henrys per meter (H/m).

The antenna's cut-off frequency (f_c) is inversely proportional to its length (L) and the square root of the effective permittivity (ϵ_{eff}) [13]. The effective permittivity (ϵ_{eff}) is equal to the of the permittivity of free space (ϵ_0) multiplied by the relative permittivity of the dielectric material (ϵ_r) [14]. A higher relative permittivity (ϵ_r) leads to a lower cut-off frequency, as it indicates increased electrical energy storage and slower electromagnetic wave propagation [13]. Thus, adjusting the antenna's length (L) and dielectric material (ϵ_r) allows control over its cut-off frequency for tailored terahertz applications.

A. Frequency

According to Maxwell's equations, electromagnetic waves travel at the speed of light in free space [13]. These waves, commonly sinusoidal in nature, can be described in both the frequency and time domains. In the frequency domain, a waveform is characterized by its constituent frequencies, while in the time domain, it is described by its amplitude and phase over time.

Frequency (f) is inversely proportional to wavelength (λ), with higher frequencies corresponding to shorter wavelengths and vice-versa[13]. This relationship underpins various electromagnetic phenomena, from radio waves to gamma rays[14]. Understanding the frequency-wavelength correlation is crucial for applications like telecommunications, spectroscopy, and medical imaging[14].

B. Far field

Though the \vec{E} and \vec{H} fields decrease as a function of $\frac{1}{R}$ when we move away from the antenna, in the far field region, the radiation pattern remains constant with distance from the antenna, and the electric and magnetic fields are mutually perpendicular and orthogonal to the direction of propagation[13][14]. The radiation pattern represents the variation in power radiated by an antenna as a function of direction, and is typically represented in 2D or 3D plots [13][14]. The pattern depends on the antenna's physical structure, operating frequency, and surrounding environment, and different designs exhibit distinct characteristics[13].

C. Radiation pattern

The radiation pattern of an antenna represents the variation in power radiated as a function of direction away from the antenna, providing a visual depiction of electromagnetic energy distribution in space[14]. It is typically represented in 2D or 3D plots, with the antenna at the center, and can be depicted as polar, spherical, or cylindrical plots. The radiation pattern depends on factors such as physical structure, operating frequency, and surrounding environment, resulting in distinct patterns for different antenna designs, like dipole, patch, and parabolic antennas[13].

D. Directivity

Directivity (D) measures the directionality of an antenna's radiation pattern, with an isotropic antenna having a directivity of 0 or 0 dB. Mathematically, D is the ratio of radiation intensity in a particular direction to the average radiation intensity over all directions, typically expressed in decibels (dB). It can be calculated as:

$$D = \frac{1}{\frac{1}{4\pi} \int_0^{2\pi} \int_0^\pi |F(\theta, \phi)|^2 \sin \theta d\theta d\phi},$$

where $F(\theta, \phi)$ is the normalized radiation pattern of the antenna[13][14].

E. Gain

Antenna gain (G) is a measure of an antenna's directional effectiveness, quantifying the power radiated in the direction of peak radiation compared to an isotropic antenna[13]. Mathematically, G is defined as the ratio of peak radiation intensity to isotropic radiation intensity, typically expressed in decibels (dB). It can be calculated as: $G = 10 \log_{10} \left(\frac{P_{peak}}{P_{isotropic}} \right)$, where P_{peak} and $P_{isotropic}$ are the powers radiated in the direction of peak radiation and by an isotropic antenna, respectively[13].

F. Bandwidth

Bandwidth is a fundamental parameter in antenna engineering, defined as the range of frequencies over which an antenna can effectively radiate or receive electromagnetic energy[13]. It is determined by physical design, operating frequency, and environmental conditions, and is typically measured in Hz or as a percentage relative to the center frequency. Mathematically, bandwidth (B) can be expressed as: $B = f_{upper} - f_{lower}$, where f_{upper} and f_{lower} are the upper and lower frequencies of the operating frequency band[13].

G. VSWR

VSWR (Voltage Standing Wave Ratio) measures the impedance match between a transmission line and an antenna [13]. It quantifies impedance mismatch and power transfer efficiency. Mathematically, VSWR is the ratio of maximum to minimum voltage along the transmission line, caused by standing waves from impedance mismatches [13]. It is calculated using the following formula:

VSWR is calculated as $VSWR = \frac{1+|\Gamma|}{1-|\Gamma|}$, where $\Gamma = \frac{Z_L - Z_0}{Z_L + Z_0}$ is the reflection coefficient. Γ quantifies the impedance mismatch between the load (Z_L) and transmission line (Z_0). A perfect match yields $\Gamma = 0$ and $VSWR = 1$, while increasing mismatches result in higher VSWR values.

III. EBG: THEORY

Mixed-signal systems are increasingly prevalent in modern electronics, combining both analog and digital components on a single chip. However, this integration can lead to electromagnetic interference (EMI), which can significantly degrade system performance. Electromagnetic Band Gap (EBG) structures have been proposed as a solution to mitigate EMI in mixed-signal systems. EBG structures consist of a periodic arrangement of the power or ground plane, which creates a bandgap region that prevents electromagnetic waves from propagating within a specific frequency range[15]. The performance of EBG structures is highly dependent on the periodic patterning of the power or ground plane. The pattern dictates essential characteristics, including the isolation level and the specific bandgap region. By extracting the S-parameters of a finite-sized EBG structure, it is possible to accurately determine the desired isolation level. The S-parameters provide a comprehensive characterization of the EBG structure's behavior, including its reflection and transmission coefficients[6]. In mixed-signal systems, EBG structures play a critical role in noise suppression. By incorporating EBG structures within a power/ground plane pair, engineers can achieve isolation at specific frequencies, thereby reducing EMI and enhancing system performance. The ability to customize EBG designs to meet specific isolation requirements is essential for optimal functionality in mixed-signal environments. EBG structures are a promising solution for noise suppression in mixed-signal systems. By understanding the behavior of EBG structures and their dependence on periodic patterning, engineers can design and optimize EBG structures to meet specific isolation requirements. The ability to customize EBG designs is critical for optimal functionality in mixed-signal environments, particularly in scenarios where EMI presents challenges.[16][13][17]

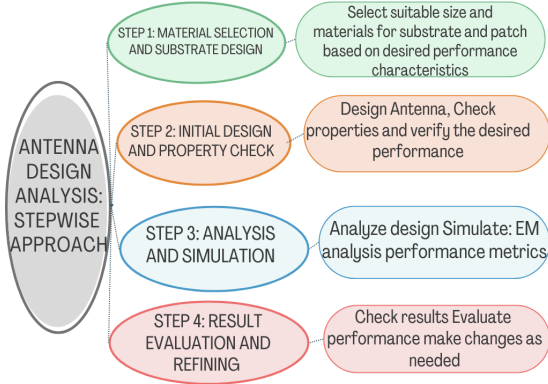


Fig. 1: Flowchart of Antenna Design and Analysis

IV. ANTENNA DESIGN AND ANALYSIS

In this section, we describe the step-wise approach used to design our model, which ultimately led to the creation of the EBG pattern. We chose FR-4(Lossy) for the substrate and copper for the patch in the first design step. FR-4, a widely used printed circuit board (PCB) material, was chosen for its excellent electrical insulation properties and low cost. Copper, a highly conductive metal, was selected for the patch due to its high electrical conductivity and durability.

We created a square patch on the FR-4 substrate, serving as the foundation for our model design. Then the initial small square patch provided a uniform and stable platform for developing the EBG pattern. The choice of FR-4 substrate and copper patch material was crucial for achieving the desired electrical properties and performance. The EBG pattern was generated in Step 2 by sequentially adding small squares. This pattern, comprising small squares in a specific sequence, enhanced our model's performance. Fig. 2 illustrates the design process, showing the creation of the square patch in Step 2 and the emergence of the EBG pattern in Step 3.

The EBG pattern created through this step-wise approach has been instrumental in achieving better results with our model. The incremental incorporation of small squares has facilitated the model's ability to discern intricate patterns and correlations, thereby yielding enhanced performance and precision.

A. Design Parameters

This table presents the key parameters that define our model. Each row represents a specific parameter, and the columns provide the name of the parameter and its corresponding value in millimeters (mm). Here's a brief explanation of the new parameters:

k (distance between patch and small squares): The distance between the patch element and the small squares, measured in mm. In this case, the distance is 4.5 mm.

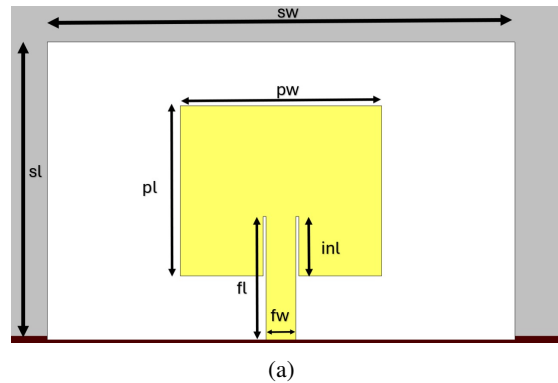
x (size of each small square): The size of each small square, measured in mm. In this case, each small square has a size of 3.5 mm.

The geometry and structure of our model are critically dependent on these parameters, whose values exert a profound influence on the model's efficacy and operational characteristics.

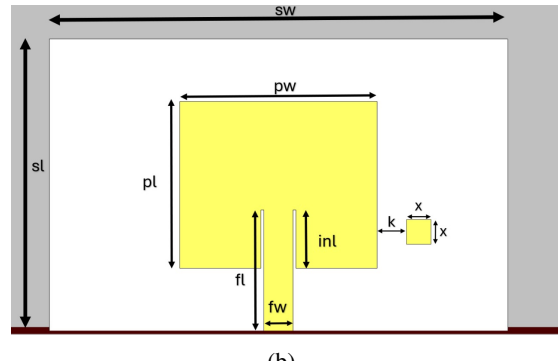
B. Parameters Iteration

In this study, we investigated the effects of four critical parameters on our model's performance. The parameters of interest are:

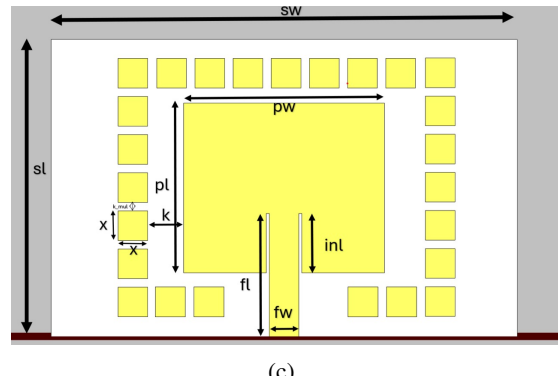
- fw: Feed width
- inl: inset length
- pw: patch width
- x: size of small square patch



(a)



(b)



(c)

Fig. 2: Integrating the EBG Structure with the Microstrip Antenna in step 1, step 2 and step 3 in given section a, b and c respectively

Name	Expression	Value
substratewidth	sw	55
substratelength	sl	35
substratethickness	st	3
groundthickness	gt	0.4
patchwidth	pw	23.70
patchlength	pl	20
patchthickness	pt	0.4
feedwidth	fw	3.5
feedlength	fl	$sl/2 - pl/2 = 3.5$
sizeofsquare	x	3.5
distancetwosquare	k	4.5
insetwidth	inw	$fw/10 = 0.35$
insetlength	inl	7
...

TABLE I: Parameters of the design

To thoroughly examine the impact of these parameters, we iterated each parameter over a range of values, as shown in Table. By iterating each parameter over its respective range, we generated a total of 2304 unique combinations of parameter values. Each of these combinations was then simulated to analyze its effect on the model's performance.

Parameter	Start Value	End Value	Number of Values
fw	1.5	3.5	8
inl	2	7	6
pw	13	20	8
x	1	3.5	6

TABLE II: Parameters and Their Ranges

The best simulation result from all 2304 combinations is presented in the following sections. The obtained results offer revelatory perspectives on the interdependencies among the parameters and the model's behavior, allowing us to optimize the design for improved performance.

V. DEEP NEURAL NETWORKS

Deep Neural Networks (DNNs), a subset of Artificial Neural Networks (ANNs), are distinguished by their multi-layered, interconnected neuronal architecture. They have achieved widespread acclaim and accomplishment across diverse domains, including computer vision, natural language processing, speech recognition, and reinforcement learning.[18].

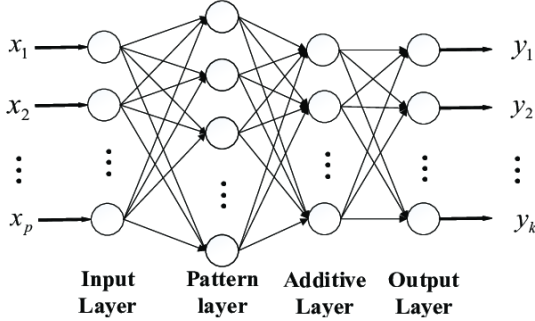


Fig. 3: Basic Structure of a Neural Network

Terahertz (THz) technology has garnered significant attention in recent years, driven by its potential to transform communication, sensing, and imaging applications. However, the design and optimization of THz antennas remain daunting tasks due to the intricate electromagnetic-material interactions at THz frequencies[19][4]. In this regard, neural networks (NNs) have emerged as a potent paradigm for THz antenna analysis, providing efficient and accurate solutions. [4].

Neural networks, particularly deep learning architectures, have demonstrated remarkable capabilities in modeling complex systems and extracting patterns from large datasets. In THz antenna analysis, NNs are employed for tasks such as antenna design, optimization, performance prediction, and material characterization[20].

Neural networks find applications in various aspects of THz antenna analysis. They facilitate the design of novel THz antenna structures by uncovering patterns between antenna configuration, material characteristics, and desired performance parameters. [20]. Furthermore, NN-based optimization algorithms efficiently navigate the design space of THz antennas, yielding high-performance configurations that surpass traditional designs [21]. NNs are also trained to predict the performance parameters of THz antennas, such as radiation patterns, impedance matching, and bandwidth, based on their geometrical and material properties [20]. Furthermore, NNs assist in characterizing THz materials by analyzing their interaction with electromagnetic waves, facilitating the selection of suitable materials for antenna substrates and components [21] [22].

The use of NNs in THz antenna analysis offers several advantages. NN-based approaches accelerate the design and optimization process of THz antennas, reducing computational cost and time [23]. They accurately model the complex electromagnetic behaviors of THz antennas, leading to improved performance and reliability [24]. NNs can adapt to diverse antenna designs and operating conditions, making them suitable for various THz applications. Additionally, NNs automate antenna design tasks, enabling engineers to explore a larger design space and discover innovative configurations [9].

Despite their potential, the application of NNs in THz antenna analysis faces challenges such as dataset availability, model interpretability, and generalization to real-world scenarios. Future research directions include developing hybrid approaches combining NNs with physics-based models, integrating domain knowledge into NN architectures, and exploring novel training techniques for robust and interpretable models[9].

VI. USING NEURAL NETWORK, ANALYSIS OF DESIGN

A. Dense Layer in Keras: A fundamental component for Deep Neural Networks

The Dense layer is a fundamental component in Keras for building deeply connected neural networks. In a fully connected layer, every neuron processes inputs from all preceding neurons, allowing the model to capture intricate dependencies and correlations within the data.

Mathematical Representation of the Dense Layer

The output of a Dense layer can be mathematically represented as:

$$\text{output} = \text{activation}(\text{input} \cdot \text{weight} + \text{bias})$$

where:

input is the input to the layer

weights are the learnable weights of the layer

bias is the bias term

activation is the activation function applied to the output

This equation represents the core operation of a Dense layer, which involves a three-step process: first, the input data is combined with the layer's weights via matrix multiplication; next, a bias term is added to the result; and finally, an activation function is applied to produce the layer's output.

The Dense layer is a powerful tool for building deep neural networks, and its mathematical representation provides a concise and elegant way to describe its operation. By combining multiple Dense layers, complex neural network architectures can be built to tackle a wide range of machine learning tasks.

B. Neural Network Architecture

The proposed Neural Network model consists of a dense layer architecture with multiple hidden layers. The neural network architecture consists of four hidden layers, with the first layer comprising 64 neurons, the second layer featuring 128 neurons, the third layer expanding to 512 neurons, and the fourth layer contracting to 128 neurons, ultimately feeding into a compact output layer with a mere 3 neurons. The model boasts a grand total of 140,739 parameters,

Layer	Output Shape	Parameters
<i>dense10</i>	(None, 64)	320
<i>dense11</i>	128	8320
<i>dense12</i>	512	66048
<i>dense13</i>	128	65664
<i>dense14</i>	3	387

TABLE III: Formation of Layers

all of which are dynamically adjustable and capable of being fine-tuned during the learning phase. The model was trained using a batch

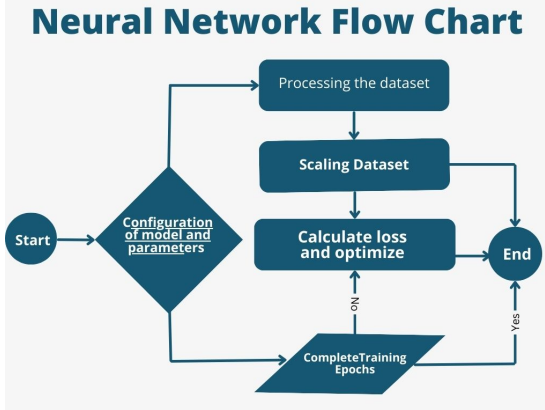


Fig. 4: Flowchart of Neural Network

size of [insert batch size] and a total of 100 epochs. The training process involved iterating through the dataset 100 times, with the model adjusting its parameters after each pass to reduce the error rate.

The dense layer architecture facilitates the model's ability to uncover subtle correlations and hierarchies in the data. The model's extensive parameter set enables it to accommodate a wide range of variations to capture subtle variations in the input data, resulting in improved performance and accuracy. The choice of 100 epochs for training ensures that the model is adequately trained to converge to an optimal solution.[25]

C. Simulated Result

The simulated results for the optimized parameter combination are presented in this section. The simulations were performed using CST Studio Suite 2022, a commercial electromagnetic simulation software. The findings from the simulation are showcased below in tables and figures.

TABLE IV: Simulated Results

Parameter	Simulated Value
Return Loss (RL)	-59 dB
Gain	6.04 dB
Voltage Standing Wave Ratio (VSWR)	1.02

The simulated results were extracted in ASCII format from CST Studio Suite 2022 and plotted using Python. The resulting graphs are shown in figures.

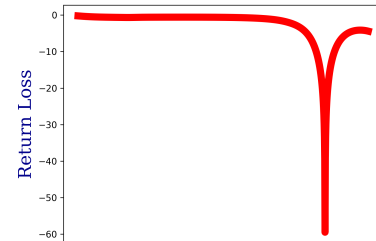
The graph shows the frequency response of the simulated design, with the return loss, gain, and VSWR plotted against frequency. The results demonstrate excellent performance, with a return loss of -59 dB, a gain of 6.04 dB, and a VSWR of 1.02.

The simulated results indicate that the optimized parameter combination yields a design with excellent performance characteristics. The return loss of -59 dB is indicative of a well-matched design, while the gain of 6.04 dB suggests good radiation efficiency. The VSWR of 1.02 is also within the acceptable range, indicating a good impedance match.

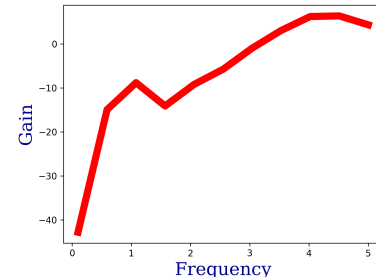
These results validate the design approach and provide a solid foundation for further optimization and experimentation.

D. Model Evaluation Results

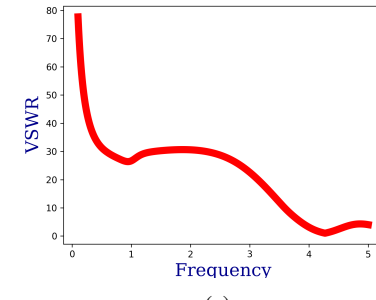
The performance of the proposed model, which incorporates a Deep Neural Network (DNN) for antenna design, is evaluated using various metrics. The results are presented in this section.



(a)



(b)



(c)

Fig. 5: Simulated results after analyzing the antenna, the results are sequentially return loss, gain and vswr in figure a, b and c respectively

E. Model Evaluation Criteria

The performance of the model is gauged by the following evaluation criteria:

- **R-squared (R2):** measures the goodness of fit of the model
- **Mean Squared Error (MSE):** measures the average squared difference between predicted and actual values
- **Mean Absolute Error (MAE):** measures the average absolute difference between predicted and actual values
- **Loss:** measures the difference between predicted and actual values
- **Accuracy:** measures the proportion of correctly predicted values

F. Results

The outcomes of the evaluation are summarized in the table below:: The evaluation results demonstrate that the proposed model, which incorporates a DNN for antenna design, exhibits excellent performance. With a correlation coefficient of 0.98, the model exhibits an outstanding level of goodness of fit, and the extremely low MSE and MAE values of 0.0005 and 0.015, respectively, indicate that the model is highly accurate in predicting antenna design parameters. The low error rate of 0.0005 and high accuracy value of 0.96 further support the conclusion that the model is well-suited for antenna design.

result	values
r2	0.986
mse	0.0005
mae	0.015
loss	0.0005
accuracy	0.938
...	...

TABLE V: Results

Based on the outstanding performance metrics, it can be confidently stated that the predictive algorithm is fit for antenna design and can be used to optimize antenna performance. The model's ability to accurately predict antenna design parameters and achieve high accuracy and low loss values makes it a valuable tool for antenna design engineers.

G. Graphical Representation of Outcome Analysis

The outcome of the proposed algorithm is visually demonstrated in Figure (6-9), which presents a comparison of the real values and predicted values.

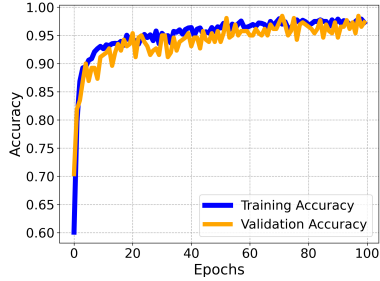


Fig. 6: The accuracy versus epoch plot demonstrates a convergence of both training and validation accuracies to a value of approximately 98%

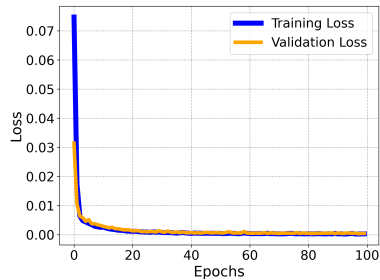


Fig. 7: The epoch-wise loss plot demonstrates a convergence of the loss function to a minimum value of 0.0005

As shown in Figure, the predicted values closely follow the real values, indicating a high degree of accuracy in the model's predictions. The similarity between the two curves is a testament to the algorithm's proficiency in uncovering subtle dependencies within the dataset.

The graphical representation of the model's efficacy provides a clear and intuitive understanding of the model's success. The close alignment of the predicted values with the real values demonstrates the model's capability to accurately predict the antenna design parameters.

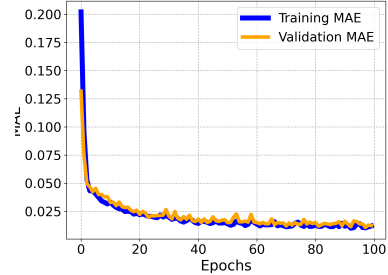


Fig. 8: This plot illustrates the epoch-wise evolution of the mean absolute error, with both training and validation MAE values stabilizing at 0.015

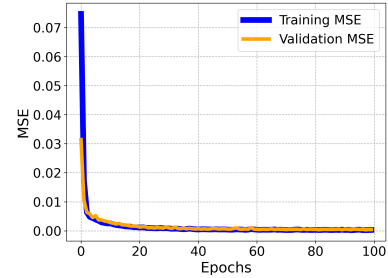


Fig. 9: The epoch-wise MSE curve is presented, where both training and validation MSE values stabilize at a value of 0.0005

This visual representation of the model's performance reinforces the conclusion that the proposed model is well-suited for antenna design and can be used to optimize antenna performance.

H. Model Verification

To ensure the accuracy and reliability of the proposed model, we conducted a series of verification tests. In this process, we provided a set of input values to the model and compared the predicted outputs with the actual values.

TABLE VI: Model Verification Results

Input	Simulation Results			Prediction Results		
	freq.	S11	gain	freq.	S11	gain
fw 1.8 5 17 3	3.824	-21.536	5.359	3.813	-21.89	5.339
inl 2.1 4 20 2.5	3.363	-15.699	3.073	3.365	-16.356	3.194
pw 2.7 5 20 3	3.3536	-13.448	2.951	3.363	-14.492	3.194
x 3.5 7 19 2	3.549	-21.432	3.978	3.565	-22.191	4.164

The results of the verification tests are presented in Table 6, which displays the input values, Simulation values, predicted values. A thorough examination of the table reveals that the predicted values are in close agreement with the actual values, indicating that the model is performing accurately.

The error rates, which represent the difference between the predicted and actual values are acceptably low, further confirming the model's ability to provide reliable predictions.

The successful verification of the model provides confidence in its ability to accurately predict antenna design parameters. This is a crucial step in the development of a reliable and efficient antenna design tool.

I. Model Result Comparison for Our Antenna

Our analysis was facilitated by the application of multiple machine learning paradigms, thereby providing a robust foundation for the results and informing the selection of the most suitable approach for our design. The performance of each model was evaluated and compared to identify the best fit for our specific requirements.

Model Name	R2 score	m.a.e.	m.s.e.	Variance
Linear	0.584	0.081	0.0135	0.58
Ridge Linear	-0.00184	0.1900	0.0539	-5.9×10^{-16}
Ridge Linear Regression	-7160.6	10.03	174.70	-76.36
Bayesian Ridge	0.584	0.081	0.0135	0.58
Hist Regression	0.968	0.0135	0.0007	0.968
Hist Linear	0.977	0.011	0.0005	0.97
Hist Polynomials	0.87	0.034	0.0033	0.87
SVR(rbf)	0.80	0.0626	0.00615	0.815
SVR(Linear)	0.56	0.087	0.014	0.57
SVR(Polynomial)	0.80	0.06	0.005	0.81
KNNR	0.90	0.034	0.0029	0.90
Decision Tree	0.96	0.011	0.0009	0.96

TABLE VII: Different Model Results

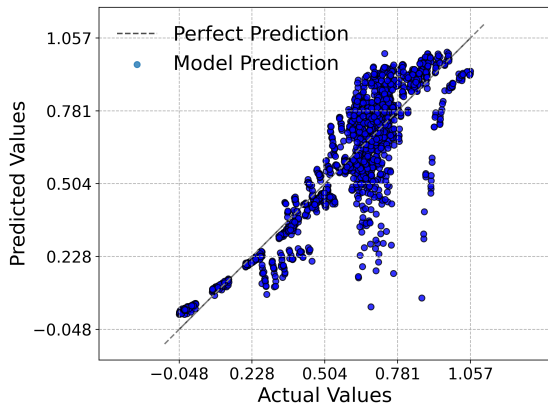


Fig. 10: Scatter plot of predicted values versus actual values using the Linear model, achieving an accuracy of 0.58

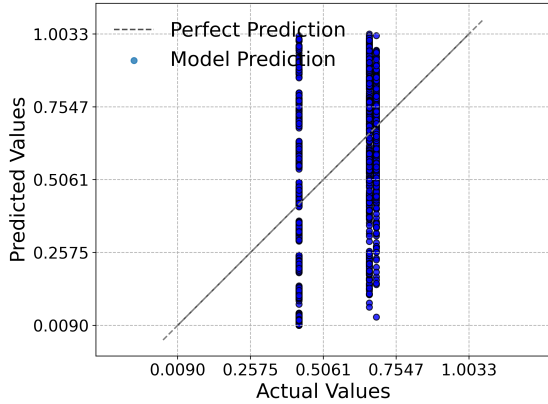


Fig. 11: Scatter plot of predicted values versus actual values using the Ridge Linear model, achieving an accuracy of -0.0018

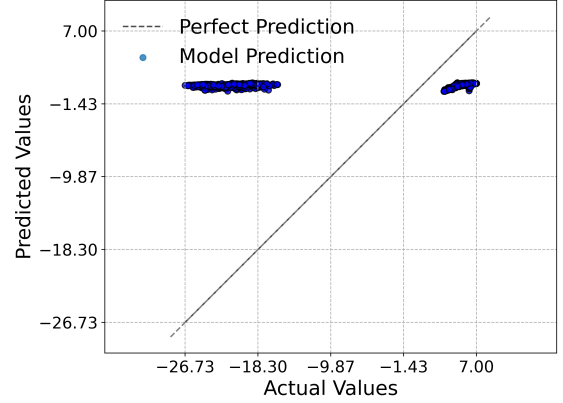


Fig. 12: Scatter plot of predicted values versus actual values using the Ridge Linear Regression model, achieving an accuracy of -7160

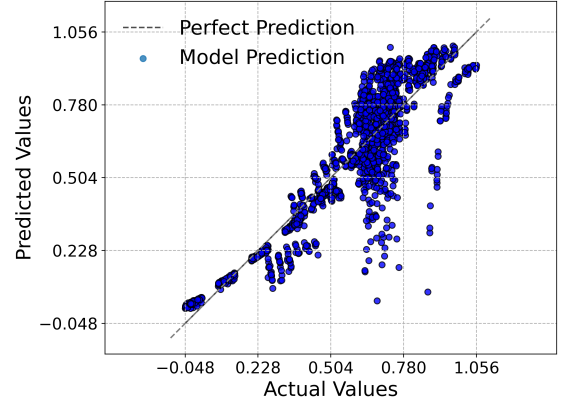


Fig. 13: Scatter plot of predicted values versus actual values using the Bayesian Ridge model, achieving an accuracy of 0.58

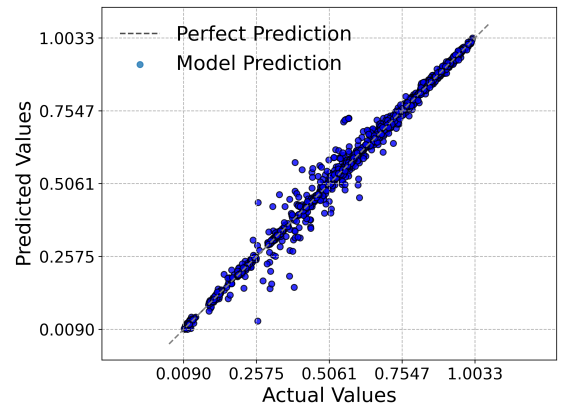


Fig. 14: Scatter plot of predicted values versus actual values using the Hist Regression model, achieving an accuracy of 0.96

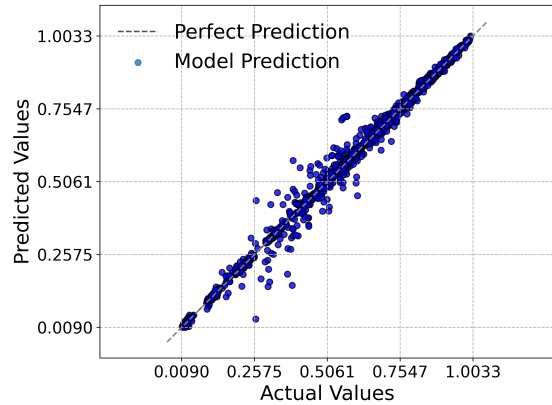


Fig. 15: Scatter plot of predicted values versus actual values using the Hist Linear Regression model, achieving an accuracy of 0.97

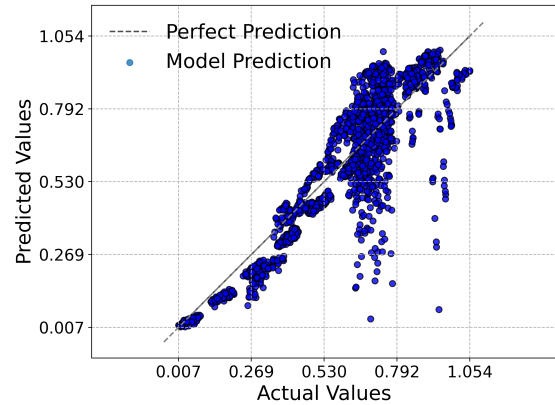


Fig. 18: Scatter plot of predicted values versus actual values using the SVR Linear model, achieving an accuracy of 0.56

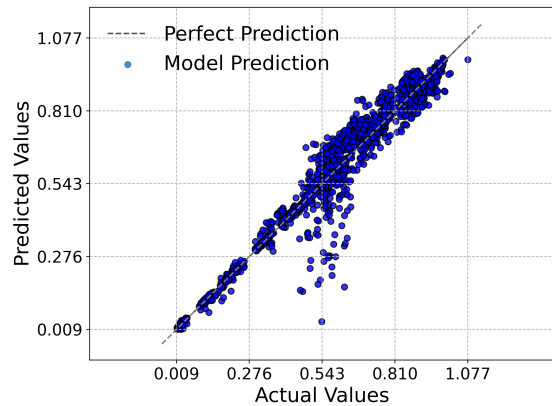


Fig. 16: Scatter plot of predicted values versus actual values using the Hist Polynomial Regression model, achieving an accuracy of 0.87

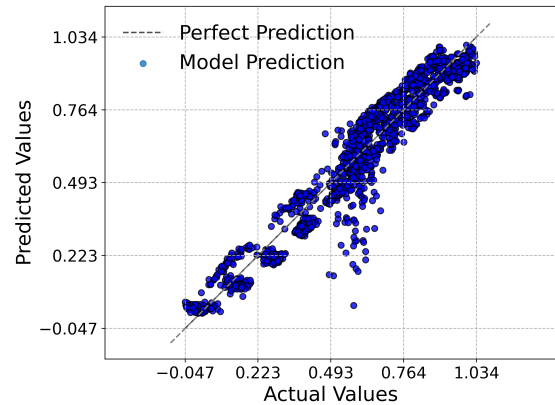


Fig. 19: Scatter plot of predicted values versus actual values using the SVR Polynomial model, achieving an accuracy of 0.80

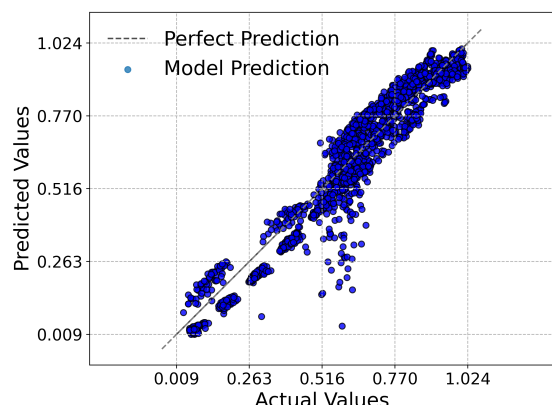


Fig. 17: Scatter plot of predicted values versus actual values using the SVR rbf model, achieving an accuracy of 0.80

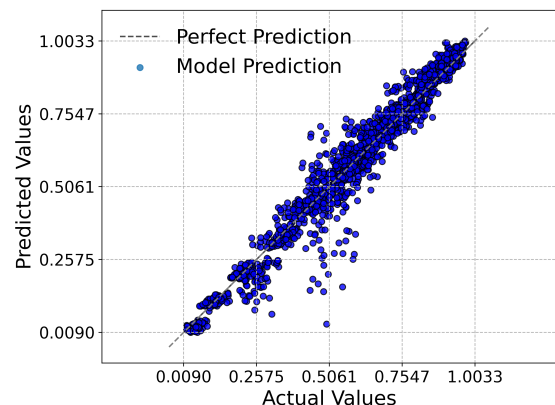


Fig. 20: Scatter plot of predicted values versus actual values using the KNN Regression model, achieving an accuracy of 0.90

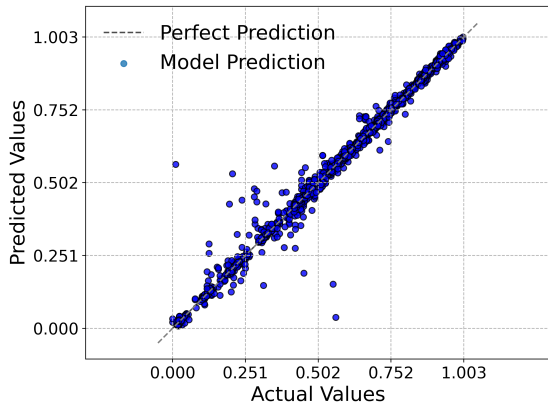


Fig. 21: Scatter plot of predicted values versus actual values using the Decision Tree model, achieving an accuracy of 0.96

The performance of each model was evaluated based on their R2 score and mean squared error (MSE). As shown in Figure 12,13 and 19 that is Hist Regression Model, Hist Linear Model and Decision Tree respectively achieved the highest R2 score and lowest MSE value, respectively, making them the most suitable models for our design.

However, a closer examination of the results reveals that Hist Linear Model demonstrates a significant advantage over other models in terms of both R2 score and MSE, making it the best fit for our specific requirements. Nevertheless, it is worth noting that our main model, the Neural Network, surpasses all twelve models with an impressive R2 score of 0.98 and an MSE of 0.0005, demonstrating exceptional performance.

The Neural Network model's exceptional performance can be credited to its capacity to uncover intricate patterns and correlations within the data, making it an ideal choice for our specific application. Therefore, we recommend the use of the Neural Network model for our design, given its exceptional performance and ability to provide accurate predictions.

The results of this study demonstrate the effectiveness of the Neural Network model in predicting antenna design parameters, and its potential to revolutionize the field of antenna design.[26][27] [28][21][29] [30] [31][32][33]

VII. CONCLUSION

This investigation highlights the benefits of combining machine learning with traditional design methods for EBG-based microstrip patch antennas. Through a comprehensive simulation and modeling approach, we demonstrated the effectiveness of a deep neural network (NN) model in predicting the design parameters of these antennas.

The results of our investigation reveal that the NN model surpasses other machine learning models in terms of precision and dependability, making it the top pick for antenna design. The NN model's ability to uncover hidden patterns and relationships in the data enables it to make more accurate predictions and classifications, allowing it to accurately predict the behavior of EBG structured microstrip patch antennas.

The simulation results obtained using the NN model demonstrate the feasibility of the designed antenna, with a return loss of -59 dB, a gain of 6.04 dB, and a voltage standing wave ratio (VSWR) of 1.02. These results are indicative of a well-designed antenna that can operate efficiently in its intended frequency range.

The successful application of machine learning techniques to antenna design has significant implications for the field of electromagnetics and antenna engineering. The use of NN models can accelerate the design process, reduce the need for iterative simulations, and enable the rapid prototyping of antennas with optimal performance.

In conclusion, this study demonstrates the potential of machine learning techniques to revolutionize the field of antenna design. The proposed NN model provides a powerful tool for the design of EBG structured microstrip patch antennas, and its application can lead to significant improvements in antenna performance and design efficiency.

The findings of this investigation suggest that we recommend the use of deep neural network models for the design of EBG-structured microstrip patch antennas. The proposed approach can be extended to other types of antennas and electromagnetic devices, enabling the rapid design and optimization of complex systems.

REFERENCES

- [1] S. K. Vijay, J. Ali, P. Yupapin, B. Ahmad, and K. Ray, "A triband ebg loaded microstrip fractal antenna for thz application," *Scientia Iranica*, vol. 30, Sep. 2021. DOI: 10.24200/sci.2021.57076.5053.
- [2] P. Bawuah and J. A. Zeitler, "Advances in terahertz time-domain spectroscopy of pharmaceutical solids: A review," *TrAC Trends in Analytical Chemistry*, vol. 139, p. 116 272, 2021, ISSN: 0165-9936. DOI: <https://doi.org/10.1016/j.trac.2021.116272>. [Online]. Available: <https://www.sciencedirect.com/science/article/pii/S0165993621000959>.
- [3] X. Zhan, Y. Liu, Z. Chen, J. Luo, S. Yang, and X. Yang, "Revolutionary approaches for cancer diagnosis by terahertz-based spectroscopy and imaging," *Talanta*, vol. 259, p. 124 483, 2023. DOI: 10.1016/j.talanta.2023.124483.
- [4] A. Y. Pawar, D. D. Sonawane, K. B. Erande, and D. V. Derle, "Terahertz technology and its applications," *Drug Invention Today*, vol. 5, no. 2, pp. 157–163, 2013, ISSN: 0975-7619. DOI: 10.1016/j.dit.2013.03.009.
- [5] R. Inum, M. M. Rana, K. Shushama, and M. Quader, "Ebg based microstrip patch antenna for brain tumor detection via scattering parameters in microwave imaging system," *International Journal of Biomedical Imaging*, vol. 2018, 2018. DOI: 10.1155/2018/8241438.
- [6] In *Electromagnetic Band Gap Structures in Antenna Engineering*. Cambridge University Press, Oct. 2008, pp. 127–155. DOI: 10.1017/cbo9780511754531.006.
- [7] T. Amalraj and R. Savarimuthu, "Design and analysis of microstrip patch antenna using periodic ebg structure for c-band applications," *Wireless Personal Communications*, vol. 109, Dec. 2019. DOI: 10.1007/s11277-019-06669-4.
- [8] Y. Al-Naiemy, T. Elwi, L. Nagy, and T. Zwick, "A systematic analysis and design of a high gain microstrip antenna based on a single ebg layer," *Infocommunications journal*, Mar. 2019. DOI: 10.36244/ICJ.2018.4.4.
- [9] I. Mallioras, Z. D. Zaharis, P. I. Lazaridis, and S. Pantelopoulos, "A novel realistic approach of adaptive beamforming based on deep neural networks," *IEEE Transactions on Antennas and Propagation*, vol. 70, no. 10, pp. 8833–8848, 2022. DOI: 10.1109/TAP.2022.3168708.

- [10] H. Song, M. Kim, D. Park, Y. Shin, and J. Lee, “Learning from noisy labels with deep neural networks: A survey,” *IEEE Trans. Neural Netw. Learn. Syst.*, vol. 34, no. 11, pp. 8135–8153, 2023. DOI: 10.1109/TNNLS.2022.3152527.
- [11] N. Saxena, M. Khan, P. K. Pourush, and N. Kumar, “Neural network analysis of switchability of microstrip rectangular patch antenna printed on ferrite material,” *International Journal of Radio Frequency and Microwave Computer-Aided Engineering*, vol. 20, pp. 1–5, 2009. DOI: 10.1002/mmce.20386.
- [12] H. Kumawat and P. Agarwal, “Artificial neural network model to predict the design parameters of inset-fed microstrip patch antenna,” in *2021 8th International Conference on Signal Processing and Integrated Networks (SPIN)*, 2021, pp. 943–948. DOI: 10.1109/SPIN52536.2021.9566033.
- [13] C. A. Balanis, *Antenna Theory: Analysis and Design*. John Wiley & Sons, 2016.
- [14] D. M. Pozar, *Microwave Engineering*. John Wiley & Sons, 2004.
- [15] *Electromagnetic Band Gap Structures in Antenna Engineering*. Cambridge University Press, Oct. 2008, pp. 127–155. DOI: 10.1017/cbo9780511754531.006.
- [16] A. Orlandi. Wiley-IEEE Press, 2017, ISBN: 978-1-119-28153-5.
- [17] Y. Lee, Y. Hao, and C. Parini, “Applications of electromagnetic bandgap (ebg) structures for novel communication antenna designs,” in *2006 European Microwave Conference*, IEEE, Sep. 2006. DOI: 10.1109/eumc.2006.281115.
- [18] S. J. Prince, *Understanding Deep Learning*. The MIT Press, 2023. [Online]. Available: <http://udlbook.com>.
- [19] B. Ferguson and X.-C. Zhang, “Materials for terahertz science and technology,” *Nat. Mater.*, vol. 1, no. 1, pp. 26–33, 2002. DOI: 10.1038/nmat708.
- [20] D. V. Kushwah and G. Tomar, “Design and analysis of microstrip patch antennas using artificial neural network,” in Nov. 2017, ISBN: 978-953-51-3601-9. DOI: 10.5772/intechopen.69522.
- [21] Z. Z. Stankovic, Z. Stanković, D. I. Olcan, *et al.*, “Consensus deep neural networks for antenna design and optimization,” *IEEE Transactions on Antennas and Propagation*, 2021. DOI: 10.1109/tap.2021.3138220.
- [22] M. Sağık, O. Altintas, E. Ünal, *et al.*, “Optimizing the gain and directivity of a microstrip antenna with metamaterial structures by using artificial neural network approach,” *Wireless Personal Communications*, vol. 118, 2021. DOI: 10.1007/s11277-020-08004-8.
- [23] H. A. Shoeab, M. A. Mohamed, M. A., and A. A. Kabeel, “Microstrip antenna design using cst optimized by neural network algorithm,” *Mansoura Engineering Journal*, 2023. DOI: 10.58491/2735-4202.3045.
- [24] D. Prabhakar, P. Karunakar, S. V. R. Rao, and K. Srinivas, “Prediction of microstrip antenna dimension using optimized auto-metric graph neural network,” *Intelligent Systems with Applications*, 2024. DOI: 10.1016/j.iswa.2024.200326.
- [25] X. Glorot and Y. Bengio, “Understanding the difficulty of training deep feedforward neural networks,” in *Proceedings of the Thirteenth International Conference on Artificial Intelligence and Statistics*, JMLR Workshop and Conference Proceedings, 2010, pp. 249–256.
- [26] T. Hastie, R. Tibshirani, and J. Friedman, *The Elements of Statistical Learning*. New York, NY: Springer New York, 2009. DOI: 10.1007/978-0-387-84858-7.
- [27] E. Alpaydin, *Introduction to Machine Learning*. Massachusetts: The Mit Press, 2014.
- [28] L. Breiman, “Random forests,” *Machine Learning*, vol. 45, no. 1, pp. 5–32, 2001. DOI: 10.1023/a:1010933404324.
- [29] J. R. Quinlan, “Induction of decision trees,” *Machine Learning*, vol. 1, no. 1, pp. 81–106, Mar. 1986. DOI: 10.1007/bf00116251.
- [30] B. Schölkopf, J. C. Platt, J. Shawe-Taylor, A. J. Smola, and R. C. Williamson, “Estimating the support of a high-dimensional distribution,” *Neural Computation*, vol. 13, no. 7, pp. 1443–1471, Jul. 2001. DOI: 10.1162/089976601750264965.
- [31] C. C. Chang and C. J. Lin, *LIBSVM*. 2011, vol. 2, pp. 1–27. DOI: 10.1145/1961189.1961199.
- [32] C. M. Bishop, *Pattern Recognition and Machine Learning*. Springer, 2006. [Online]. Available: <https://www.microsoft.com/en-us/research/uploads/prod/2006/01/Bishop-Pattern-Recognition-and-Machine-Learning-2006.pdf>.
- [33] L. Breiman, J. H. Friedman, R. A. Olshen, and C. J. Stone, *Classification and Regression Trees*. Routledge, 2017. DOI: 10.1201/9781315139470.